CALCULATION OF SLIP ENERGY RECOVERY INDUCTION MOTOR DRIVE BEHAVIOR USING THE EQUIVALENT CIRCUIT

P.Pillay
Dept. of Elec. Eng.
University of New Orleans

L.Refoufi
Institut National D'Electricite
Algeria

ABSTRACT

A transformer-type equivalent circuit model for the calculation of the steady state performance of a slip energy recovery induction motor drive with a step down chopper in the dc link is described. Experimental data of rms currents, power, reactive power and overall efficiency satisfactorily correlate with calculations over most of the operating speed range. Also, detailed calculations of rotor, stator and supply harmonic currents due to the rectifier and inverter actions are performed using the conventional version of the equivalent circuit. The computed and measured instantaneous current waveforms show satisfactory agreement except at a slip of 1/6 where significant deviations appear. This effect is adequately catered for by using a more rigorous model.

1. Introduction

The simplicity of the conventional slip energy recovery induction motor drive (SERIMD) belies the degree of difficulty of its analysis. This is largely due to the interdependence between the rotor bridge rectifier conduction sequences and the rotor voltage and current waveforms. The performance of the conventional SERIMD can be enhanced by inserting a step-down chopper between the rotor rectifier and inverter in a SERIMD as shown in figure 1. While the chopper is operational, it can be used to match the rotor voltage to that of the inverter. The inverter can thus operate at its maximum safe firing angle to minimize VAR requirements. Once the chopper is fully on, inverter control can be used to control the motor up to rated speed. Hence the speed is controlled in two stages, chopper control from the minimum speed to an intermediate speed and inverter control from there to rated speed. The chopper can be used to start the drive from rest thus eliminating the three phase resistance starter. It also allows a lower turns ratio in the recovery transformer thus reducing the magnitude of harmonic currents injected into the supply.

A rigorous analysis should yield a solution that takes account of the nonsinusoidal nature of both the rotor current and voltage waveforms and all the voltage and current ripples in the system. To this end, a coupled approach (a dq/abc derived model) becomes necessary. This has been the object of several papers [1-3]. On the other hand, several methods for the steady state analysis of the conventional static Kramer drive, which are based on a non-coupled circuit approach, have been reported in the literature. The so called dc equivalent circuit (EC) approach [4] and the ac EC approach [5] are simplified methods which consist in essence, of transferring the system parameters on to the diode bridge dc or ac sides respectively. The aim of the steady state EC approaches is to calculate the overall drive performance to a sufficient accuracy that the results are usuable while avoiding the mathematical and numerical complexities of the detailed model [1-3]. They are however inherently unable to take into account the effect of motor and rectifier resistances and voltage drops on the commutation process in the diode bridge. This effect becomes substantially important at high speeds where slip and rotor voltages are low. Because of these drops in the rotor circuit, commutation will start earlier than the normal voltage crossover point and the overlap angle will be longer.

A mathematically exact steady state analysis of the drive has been done [6] which takes into account motor resistance and rectifier losses on the commutation in the diode bridge rectifier. A similar approach using a transformer-type model for the motor and based on the fundamental component of rotor and stator currents has been developed [7]. Analytical expressions for predicting torque, stator power, stator reactive power and rectifier output voltage were presented for a conventional SERIMD. In this paper, this model is extended to calculate the performance of a chopper-controlled SERIMD. In addition the conventional form of the EC is used for more detailed calculations of stator, recovery, and supply currents for a chopper-controlled drive. The paper is organized as follows: Section 1 has the

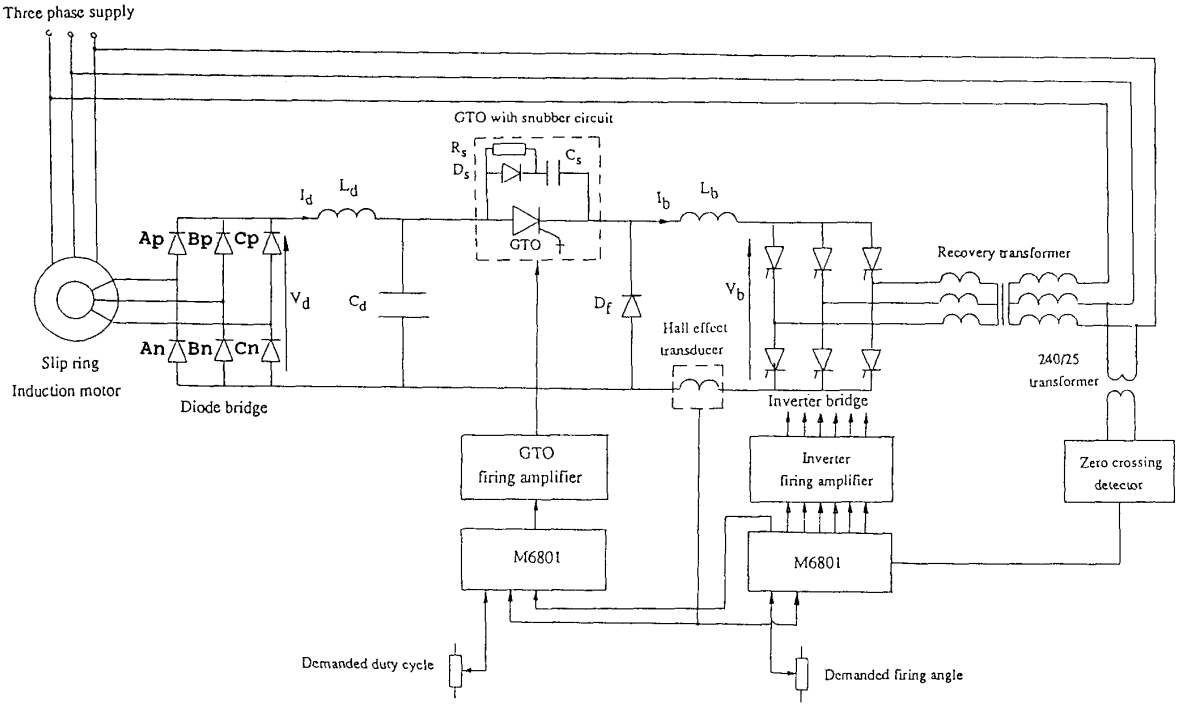

Figure 1 Step-down chopper-controlled slip energy recovery drive

0-7803-0634-1/92$03.00 ©IEEE

introduction. Sections 2 and 3 present the transformer-type EC and the steady state results for the drive. Sections 4 and 5 show how the conventional EC can be used to calculate the harmonic currents. Section 6 has the conclusions.

2. Transformer-type Circuit Model for the Induction motor

2.1 Introduction

The motor is represented by its so called transformer-type EC [8] (with all three phases treated as separate entities). The few parameters used can all be measured experimentally. This relatively unused variant of the EC has been chosen because it has the advantage of leading to a simple sinusoidal source with a series impedance for rectifier calculations while preserving the fundamental component of no load current. Figs. 2(a) and (b) compare the conventional and transformer-type ECs and show how the parameters of the latter can be derived from the former. K is a complex ratio which includes the phase shift between V_1 and V_1' on no load. The circuit is valid for the fundamental component of current only as the true equivalent circuit must differ for each harmonic. The circuit is therefore approximate since rotor current is necessarily nonsinusoidal. All current and voltage ripple in the dc link are assumed to be negligible ie, the switching actions of the chopper and inverter are neglected. It is therefore assumed that the principal harmonics impressed on the rotor circuit are simply odd multiples of slip frequency (excluding the triplen harmonics) which are caused by rectification taking place in the rotor diode bridge.

2.2.Analysis

The derivation of the formulae pertaining to the motor/diode bridge circuit are given in reference [9] and used in this analysis. Performance is calculated for given values of speed and rectifier output current I_d. However, in order to predict the performance for a specified torque/speed characteristic, because of the overlap effect in the rectifier, preliminary calculations are needed to establish the magnitude of the rectifier output current I_d required for a given torque T at a given speed. This overlap effect can go through different stages or modes. The most common mode of overlap is characterized by an overlap angle μ of less than $\pi/3$ with two and three diodes alternately conducting. This is the so called mode 1 overlap. Mode 2 overlap takes place when μ becomes equal to $\pi/3$ wherein there are three diodes conducting at any time. Under most steady state conditions, practical systems would normally experience mode 1 overlap and only occasionally mode 2 [9]. The relevant mode of overlap under any load condition has to be established first. For this purpose, the value of the rotor rectified current, called I_{d12}, at which the transition between mode 1 and mode 2 takes place can be calculated from the following equation:

$$I_s\{\mathrm{Sin}(\theta+\beta)e^{\pi D/3}-\mathrm{Sin}(\theta+\beta-\pi/3)\} = I_{d12}(1+e^{\pi D/3}) \qquad (1)$$

where:
$I_s = V/\sqrt{[R^2 + (swL_s)^2]}$
$V = \sqrt{2}.\sqrt{3}.V_s$ (peak line-to line voltage)
$\theta = \tan^{-1}(swL_s/R)$
$D = -R/swL_s$
$R = R_s + R_f$

where R_s is the resistive component of Z_s (fig. 3) and R_f is the diode forward resistance.

$$\beta = \sin^{-1}(RI_d/V) \qquad (2)$$

By comparing the rectified rotor current I_d with I_{d12} the relevant mode of overlap can then be determined. The overlap angle μ for that given value of I_d can be worked out from the following equation [9]:

$$I_s\{\sin(\theta+\beta)e^{\mu D} - \sin(\theta+\beta-\mu)\} = I_d(1+e^{\mu D}) \qquad (3)$$

The rotor current can now be described over one complete cycle [7] (fig. 3), assuming a smooth dc link current but extended to include the characteristics of the conducting diodes. The diodes are modelled as a constant voltage V_f in series with a resistance R_f. i_a (which only needs to be defined over half a cycle) can be seperated into four periods: the first is when it rises and commutation is still in progress; the second is when it is constant at the dc link value; the third is when

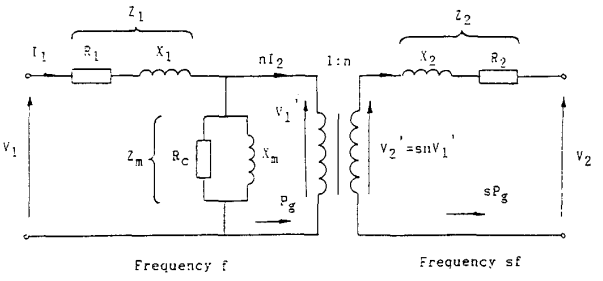

Figure 2a. Conventional induction motor equivalent circuit

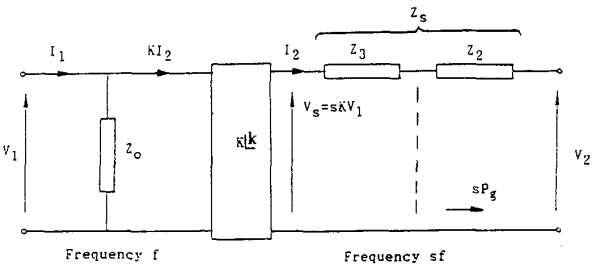

sP_g recovered power

$Z_s = Z_2 + Z_3$ $\qquad Z_o = Z_1 + Z_m$

$K = aZ_m/(Z_1+Z_m)$ $\qquad Z_3 = sa^2Z_1Z_m/(Z_1+Z_m)$

Figure 2b. Transformer-type induction motor equivalent circuit

it falls to zero and the fourth is when it is zero. The effect of the source inductance is to advance the turn-on of diode Ap given by (2). During the first period of overlap between Ap and Cp, i.e. for

$(\pi/6-\beta) \leq swt \leq (\pi/6-\beta+\mu)$,

$$i_a = [I_d + I_s\sin(swt-\theta-\pi/6) + e^D(swt+\beta-\pi/6)(I_s\sin(\beta+\theta)-Id)]/2 \qquad (4)$$

$\theta = \tan^{-1}(sw_sL_s/R)$

During the second period,

$(\pi/6-\beta+\mu) < swt \leq (5\pi/6-\beta)$

Ap conducts alone in the top row of the diode bridge and

$$i_a = I_d. \qquad (5)$$

During the second overlap period when the current transfers from Ap to Bp i.e.

$(5\pi/6-\beta) < swt \leq (5\pi/6-\beta+\mu)$

$$i_a = [I_d - I_s\sin(swt-\theta-5\pi/6) - e^D(swt+\beta-5\pi/6)(I_s\sin(\beta+\theta)-Id)]/2 \qquad (6)$$

In the final period,

$(5\pi/6-\beta+\mu) < swt < (7\pi/6-\beta)$

$$i_a = 0. \qquad (7)$$

From the above piecewise curves describing i_a, the Fourier series can be calculated from:

$$i_a(swt) = a_o + a_n\cos(nswt) + b_n\sin(nswt) \qquad (8)$$

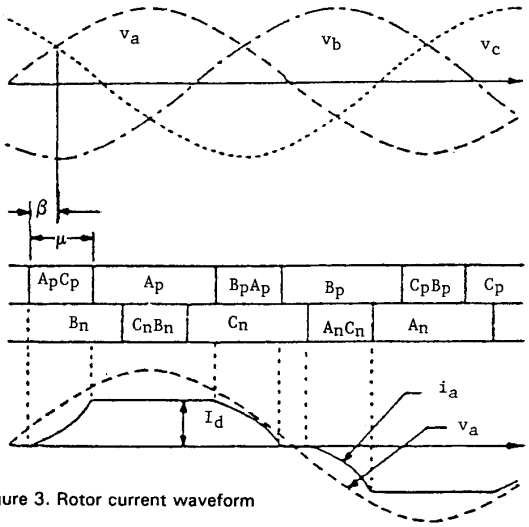

Figure 3. Rotor current waveform

where the coefficients a_o, a_n and b_n are the dc, quadrature and in-phase components of the function respectively.

$$a_o = 0 \quad (9)$$

$$a_n = 2/(T/2) \int_{\pi/6-\beta}^{7\pi/6-\beta} i_s \cos(nswt)dswt \quad (10)$$

$$b_n = 2/(T/2) \int_{\pi/6-\beta}^{7\pi/6-\beta} i_s \sin(nswt)dswt \quad (11)$$

The rms values of the quadrature and in-phase components of the fundamental rotor current (half range series) are therefore given by:

$$a_1 = \sqrt{2}/\pi \int_{\pi/6-\beta}^{7\pi/6-\beta} i_s \cos(swt)dswt \quad (12)$$

$$b_1 = \sqrt{2}/\pi \int_{\pi/6-\beta}^{7\pi/6-\beta} i_s \sin(swt)dswt \quad (13)$$

The quadrature and in phase components of the fundamental rotor current a_1 and b_1 can be shown to be equal to:

$$a_1 = \sqrt{(3/2)}(1/\pi)\{2I_d\cos(\mu/2)\sin(\beta-\mu/2) - (I_s/2)[\mu\sin\theta + \sin\mu\sin(2\beta+\theta-\mu)] + \sin\theta[I_s\sin(\theta+\beta) - I_d][\cos(\theta-\beta) - I_d - e^{D\mu}\cos(\theta-\beta+\mu)]\} \quad (14)$$

and

$$b_1 = (\sqrt{3/2})(1/\pi)\{2I_d\cos(\mu/2)\cos(\beta-\mu/2) + (I_s/2)[\mu\cos\theta + \sin\mu\cos(2\beta+\theta-\mu)] + \sin\theta[I_s\sin(\theta+\beta) - I_d][\sin(\theta-\beta) - e^{D\mu}\sin(\theta-\beta+\mu)]\} \quad (15)$$

The total r.m.s value c_1 of the fundamental rotor current and the phase angle ϕ_1 by which c_1 lags V_s can then be obtained:

$$c_1 = (a_1^2 + b_1^2)^{1/2} \quad (16)$$

$$\phi_1 = \tan^{-1}(a_1/b_1) \quad (17)$$

The average rectifier output voltage V_d obtained by integrating the instantaneous voltage that appears across the dc terminals of the diode bridge over one-sixth of a rotor cycle can be shown to be given by the following equation (mode 1):

$$V_d = (3V/\pi)\{\cos\beta - \sin(\mu/2)\sin((\mu/2)-\beta)\} - (3RI_d/\pi)(2\pi/3-\mu/2) - 2V_f \quad (18)$$

This voltage V_d will be stepped down or stepped up to the constant inverter voltage which is determined by the firing angle adjustment and the recovery transformer turns ratio.

For a step down chopper:

$$V_b/V_d = \delta \quad (19)$$

and $$I_d/I_b = \delta \quad (20)$$

For a step up chopper:

$$V_d/V_b = 1-\delta \quad (21)$$

and $$I_b/I_d = 1-\delta \quad (22)$$

where δ is the duty cycle (mark space ratio) of the chopper. For a complete modeling of the system, the characteristics of the recovery inverter are included. The approach is similar to that used for the motor/rectifier circuit except that the frequency is now equal to the supply line frequency. The average value of the dc side line commutated inverter voltage V_b is solely determined by the thyristor inverter firing angle and the transformer turns ratio if overlap in the inverter is neglected. In the chopper control mode, when the voltage V_b is kept constant,the average value of dc inverter current I_b is determined by chopper duty cycle δ and the rectified rotor current I_d. The presence of some overlap effect in the inverter may necessitate an increase in the advance firing angle in order to keep V_b constant at the value initially fixed. This second order effect was however found to be negligible. In the inverter control mode, once the required value for the back emf V_b is known for a given rectified rotor current I_d, the inverter firing angle can be determined together with the inverter real and reactive powers which can be combined with those at the stator to give the overall system characteristics.

The air-gap power P_g per phase obtained at the point shown in fig.2b is:

$$P_g = (V_s c_1 \cos\phi_1 - c_1^2 R_3)/s \quad (23)$$

where R_3 is the resistive component of Z_3 and s is the p.u. slip. The torque per phase can then be obtained from :

$$T = P_g/pw \quad (24)$$

where p is the number of pole pairs and w the ac supply frequency.

When c_1 is referred to the stator, c_1' lags V_1 by an angle (ϕ_1-2k). Adding the contribution from the Y_o term to those from c_1', the fundamental stator power P_s and reactive power Q_s per phase are then given by :

$$P_s = V_1 c_1' \cos(\phi_1-2k) + V_1^2 G_o \quad (25)$$

$$Q_s = V_1 c_1' \sin(\phi_1-2k) + V_1^2 B_o \quad (26)$$

The stator displacement factor or fundamental stator power factor pf_1 is then given by:

$$pf_1 = P_s/(P_s^2 + Q_s^2)^{1/2} \quad (27)$$

3. Experimental Verification

Measurements of real power, reactive power and currents at different points in the circuit made over a wide speed range compared well with the predicted performance. A constant torque load of 20.5 Nm with a chopper frequency of 600 Hz is used with the drive under chopper control from zero speed to 800 rpm and under inverter control from 800 rpm to 1400 rpm. The continuous line is the predicted values while the measurements are shown dotted at discrete intervals.

Figures 4(a), (b) and (c) show the supply, stator and recovery rms currents from zero up to 1400 rpm. The supply current shows a small decrease while under chopper control up to 800 rpm and then shows a small increase as the speed increases while under inverter control.

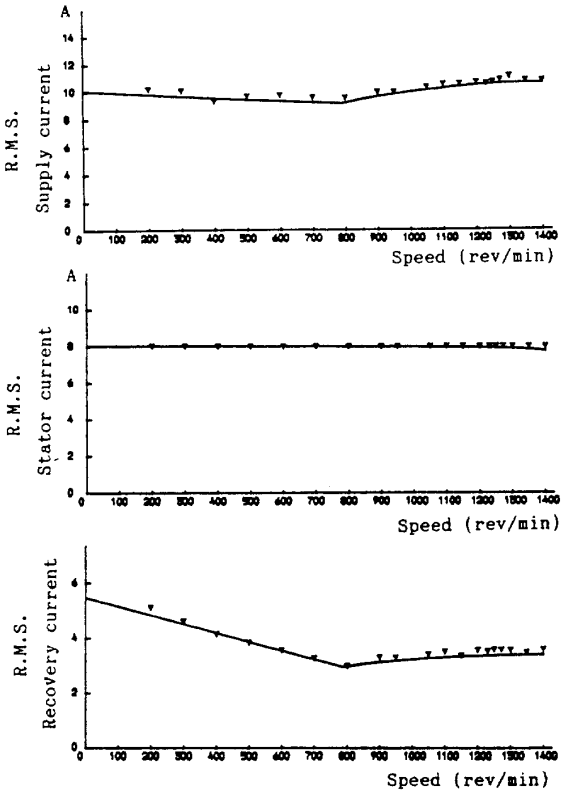

Figure 4. Drive rms currents

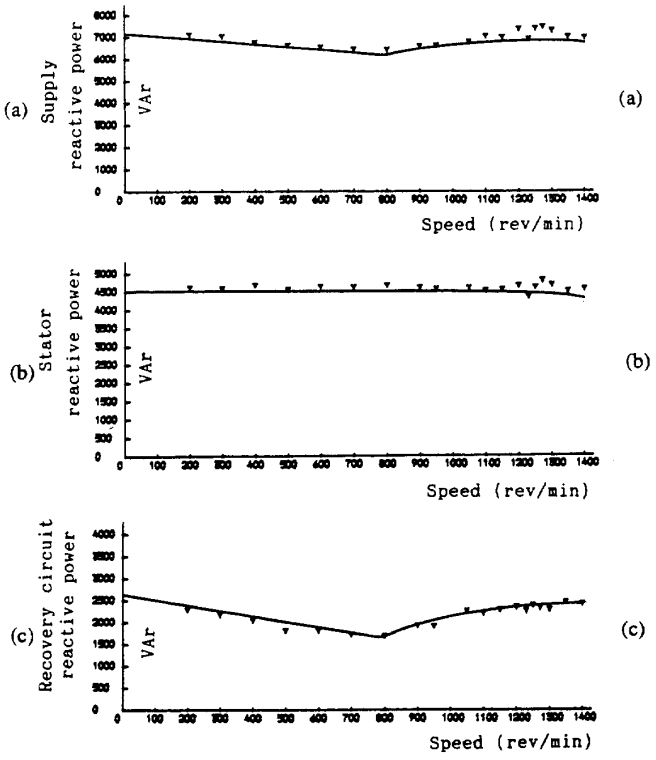

Figure 6. Reactive power of drive

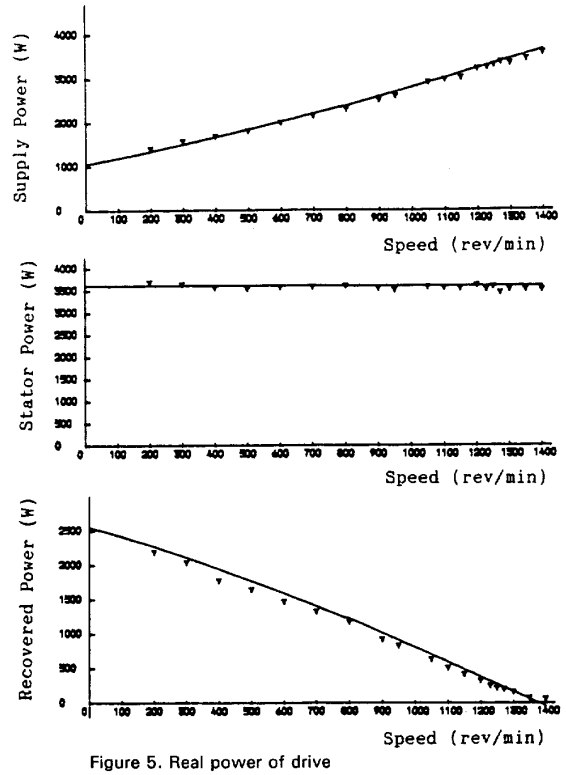

Figure 5. Real power of drive

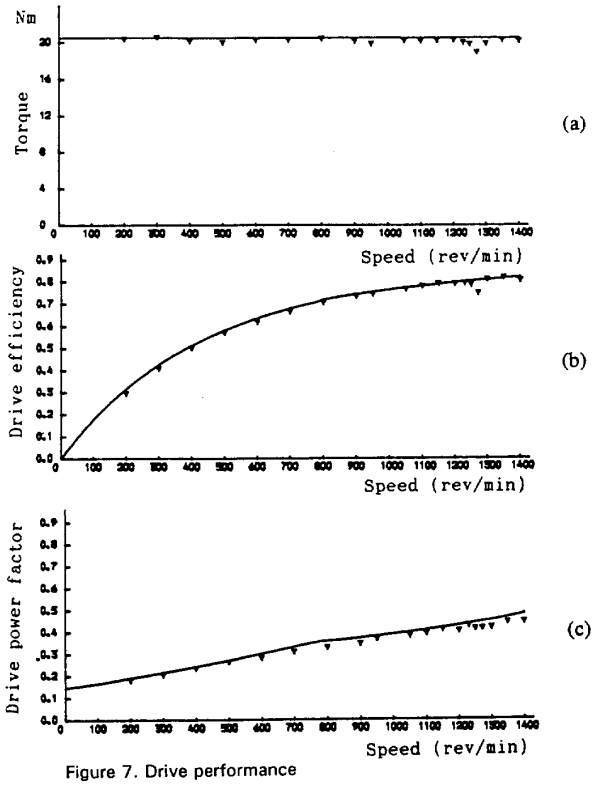

Figure 7. Drive performance

The rms stator current is approximately constant. The recovered current shows a sharp drop while under chopper control as the speed increases and then shows a more gradual increase as the speed increases under inverter control.

Figures 5 (a), (b) and (c) show the real powers of the supply, stator and the recovery circuits respectively. Because the torque is constant, the output power and supply power increases with speed. Also, as the inverter is fired at an angle approaching 90°, the recovered power goes to zero, thus resulting in a net increase in the supply power.

Figures 6 (a), (b) and (c) show the reactive powers of the supply, stator and the recovery circuits. The recovery reactive and supply reactive powers increase during an increase in speed during inverter control because the firing angle is approaching 90°.

Figures 7 (a), (b) and (c) show the torque, drive efficiency and power factor. The drive efficiency increases with speed, which follows from the motor performance. The drive power factor shows a steady increase with speed even during inverter control. The rate of increase during inverter control is however lower than during chopper control. Discrepancies between the measurements and the predicted values are essentially due to the fact that all voltage and current ripples caused by the chopper and inverter have been neglected.

The analysis is however fundamentally unable to predict the drive performance in the vicinity of a speed of 1250 rev/min where a peculiar harmonic effect takes place in the machine [9]. This effect is adequately catered for by a more rigorous model developed in [3]. Results shown here indicate that the model is accurate in predicting steady state drive performance over most of the operating speed range provided the effects of current and voltage ripples are negligible.

4. Harmonic analysis

4.1 Rotor harmonic currents

The frequencies of the rotor current harmonics resulting from rotor rectifier action are given by:

$$f_r = n.s.f \qquad (28)$$

where n is the ordinal number of the harmonic and takes integer values -5, +7, -11, +13 etc., s is the p.u. slip, and f the supply frequency. The negative sign indicates a negative sequence rotor current harmonic ie, the harmonic generated field rotates in the opposite direction to that of the fundamental. A positive sign indicates that the harmonic generated field rotates in the same direction to that of the fundamental. The in-phase and quadrature components of the n^{th} rotor current harmonics can be shown to be given by:

$$a_n = (\sqrt{2}/\pi)\sin(n\pi/3)\{(2I_d/n)\cos(n\mu/2)\cos[(\pi/2-\beta+\mu/2)n] + [I_s/(1-n)]\{\sin[(1-n)\mu/2]\cos[(-\beta+\mu/2)(1-n)-\theta-n\pi/2]\} - [I_s/(1+n)]\{\sin[(1+n)\mu/2]\cos[(-\beta+\mu/2)(1+n)-\theta+n\pi/2]\} - (1/n)\sin(\theta_n)[I_d+I_s\sin(-\beta-\theta)]\{\sin[(\pi/2-\beta)n+\theta_n] - e^{D\mu}\cos[(\pi/2-\beta+\mu)n+\theta_n]\}\} \qquad (29)$$

$$b_n = (\sqrt{2}/\pi)\sin(n\pi/3)\{(2I_d/n)\cos(n\mu/2)\sin[(\pi/2-\beta+\mu/2)n] - [I_s/(1-n)]\{\sin[(1-n)\mu/2]\sin[(-\beta+\mu/2)(1-n)-\theta-n\pi/2]\} + [I_s/(1+n)]\{\sin[(1+n)\mu/2]\sin[(-\beta+\mu/2)(1+n)-\theta+n\pi/2]\} + (1/n)\sin(\theta_n)[I_d+I_s\sin(-\beta-\theta)]\{\cos[(\pi/2-\beta)n+\theta_n] - e^{D\mu}\cos[(\pi/2-\beta+\mu)n+\theta_n]\}\} \qquad (30)$$

$$\text{where } \theta_n = \tan^{-1}(nswL_s/R) \qquad (31)$$

$$\text{and } \theta = \tan^{-1}(sw_sL_s/R) \qquad (32)$$

Triplen harmonics are absent from the AC line current waveform (three-wire system). The rms value of the n^{th} current harmonic with its corresponding relative phase shift are given by:

$$c_n = (a_n^2 + b_n^2)^{1/2} \qquad (33)$$

$$\phi_n = \tan^{-1}(a_n/b_n) \qquad (34)$$

4.2 Stator current harmonic distortion

The rotor current harmonics are reflected into the stator winding and fed into the mains at frequencies given by:

$$f_s = f[1+(n\pm1)s] = f[1\pm6ks] \qquad (35)$$

where k = 1, 2, 3 etc..

The upper and lower indices correspond to the positive and negative sequence harmonics respectively. For subsynchronous operation, the slip is determined by the following inequality:

$$1 \geq s \geq 0 \qquad (36)$$

Therefore, the frequency of the rotor-induced stator currents is normally not an integral multiple of the fundamental stator (supply) frequency. These are not, by definition, harmonics of the supply frequency but subharmonics. Given the amplitude and the phase angle of the n^{th} rotor current harmonic, the amplitude and phase angle of the rotor induced stator harmonic current can be obtained by using the motor equivalent circuit that is valid for that particular harmonic. Assuming a symmetrical machine connected to an infinite or near infinite bus with zero or negligible impedance, the stator circuit can be viewed as a short-circuit as far as the harmonics are concerned since the stator voltage is assumed perfectly sinusoidal. The rotor circuit which is the (harmonic) source is taken here as the primary winding; therefore the harmonic equivalent circuit is as depicted in fig.8 where s_n, the harmonic slip, is derived from the definition of the slip in general and found to be given by:

$$s_n = [1\pm(n\pm1)s]/n.s \qquad (37)$$

The upper and lower indexes correspond to the positive and negative sequence harmonics respectively. From the harmonic equivalent circuit of fig.8, the harmonic stator current I_{sn} that is induced by the nth rotor current harmonic I_{rn} is given by:

$$I_{sn} = I_{rn}jX_m'ns/[R_1'/s_n + j(X_m'ns + X_1's_n)] \qquad (38)$$

from which the amplitude and the phase angle of the stator harmonic currents can be found for different values of slip. The lower harmonic components such as the 5th and the 7th harmonics will have a dominating effect. Each harmonic component in the rotor will set up a magnetic field whose direction of rotation depends on the order of the harmonic. The 5th harmonic current at a frequency $5sN_s$ will rotate opposite to the direction of the rotor whereas the 7th harmonic at a frequency $7sN_s$ will rotate in the same direction. Consider the effect of the 5th harmonic. The rotor rotates at a speed $N_r = N_s(1-s)$ and the 3 phase 5th harmonic rotor currents will set up a magnetic field in the air-gap which will rotate with respect to rotor at a speed $-5sN_s$. Since the rotor is rotating at a speed $N_s(1-s)$, the resulting speed of the 5th harmonic wave with respect to the stator is $[N_s(1-s) + (-5sN_s)] = N_s(1-6s)$. The rotor induced stator current is therefore at a frequency (1-6s)f. A per-phase equivalent circuit (drawn with respect to the rotor) and valid only for the 5th harmonic is shown in fig.9. The rotor-injected harmonic current will be distributed in parallel between the stator and the magnetic circuit, hence:

$$I_5 = I_{r5}\,5sX_m'/[(5sX_m'+5sX_1')^2 + (5sR_1'/(1-6s))^2]^{1/2} = (I_n/5)X_m'/[(X_m'+X_1')^2 + (R_1'/(1-6s))^2]^{1/2} \qquad (39)$$

where I_{rf} is the fundamental rotor current.

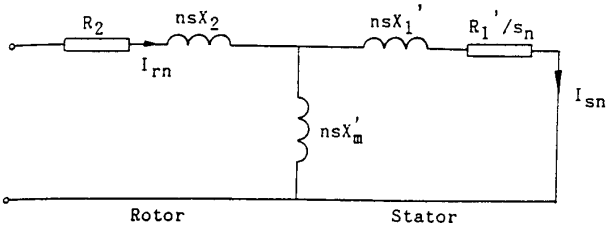

Figure 8. Harmonic equivalent circuit

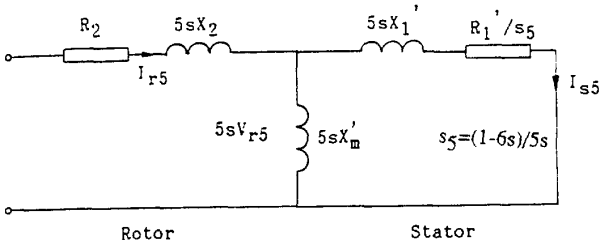

Figure 9. 5th harmonic equivalent circuit

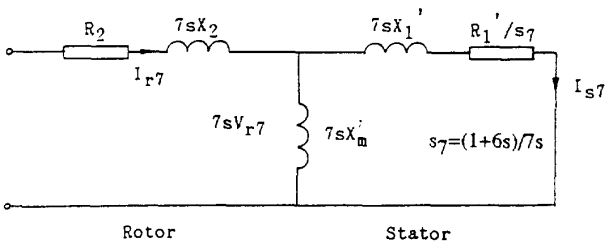

Figure 10. 7th harmonic equivalent circuit

Equation 39 suggests that the stator 5th harmonic current I_s is maximum at unity slip and zero at slip s = 1/6 which for a 4 pole machine corresponds to a speed equal to 1250 rev/min. It then increases as slip is further reduced; the equation also indicates that the induced stator harmonic is smaller than the rotor component and that its frequency which varies with slip is generally not an integer multiple of the stator frequency. This will create a variable frequency, variable amplitude beating effect on the stator current except at slips that are exactly integer multiple of the supply frequency where no such effect will appear. The 3-phase 7th harmonic rotor currents will set up a magnetic field in the air-gap which will rotate with respect to rotor at a speed of $7sN_s$ and since the rotor speed is equal to $N_s(1-s)$, the resulting speed of the 7th harmonic wave with respect to the stator is $N_s(1-s) + 7sN_s$ that is $N_s(1+6s)$. The rotor induced stator current harmonic is therefore at a frequency of $(1+6s)f$. A per-phase 7th harmonic equivalent circuit drawn with respect to the rotor is shown in fig.10. The rotor injected harmonic current will be distributed in parallel between the stator and the magnetic circuit and hence:

$$I_7 = I_{r7}\, 7sX_m'/[\{7sX_m' + 7sX_1')^2 + \{7sR_1'/(1+6s)\}^2]^{1/2} = I_{rf}X_m'/7[\{X_m' + X_1')^2 + \{(R_1'/(1+6s)\}^2]^{1/2} \quad (40)$$

where I_{rf} is the fundamental rotor current. At a slip s=-1/6, equation 40 suggests that I_7 is equal to zero and at s = 0 it is maximum and given by the following equation:

$$I_7 = I_{rf}X_m'/7[X_m' + X_1')^2 + R_1'^2]^{1/2} \quad (41)$$

Following the individual calculation of stator current harmonic components, these are then summed up with the fundamental stator current I_{s1} in order to construct the stator current waveforms. I_{s1} is readily obtained from fig.1 as:

$$I_{s1} = kI_{r1} + V_1/X_m \quad (42)$$

$$\text{or } I_1 = c_t' + I_m \quad (43)$$

4.3 Recovery current harmonic components

The in-phase and quadrature components of the n^{th} inverter current harmonics can be obtained by replacing $(-\beta)$ in equations (29) and (30) by α, the firing angle, with θ and θ_n being equal to $\tan^{-1}(wL_s/R)$ and $\tan^{-1}(nwL_s/R)$ respectively. The instantaneous value of the non-sinusoidal current drawn by the recovery inverter can therefore be obtained by summing up the fundamental component of recovery current with as many harmonic current components as deemed necessary. Knowing the fundamental and harmonic components of both the stator and inverter currents, the instantaneous value of the supply current can therefore be obtained.

5. Experimental Verification

5.1 Operation at 1300 rev/min

Fig. 11 shows the predicted stator, supply and rotor currents waveforms together with their measured counterparts at 1300 rev/min for a constant dc link current of 18 A. The stator current pulsations at a frequency of 10 Hz are clearly shown in both the predicted and measured waveforms. It appears that the effect of rotor current or voltage ripple existing in the system is not substantial as the predicted and measured stator and supply current waveforms show satisfactory agreement. On the other hand, the ripple effect on the measured rotor current waveform is very evident. There is also low frequency ripple (at slip frequency) caused by the rotor rectifier bridge voltage that is superimposed on the high frequency ripple (six times the supply frequency) caused by the inverter voltage ripple. These effects can not of course be predicted by this model. The overlap angle of the measured and predicted waveforms show reasonably close agreement.

5.2 Operation at 1250 rev/min

Figs. 12 shows the same currents at 1250 rev/min for a dc link current of 18 A. As expected, no pulsations appear on the stator and supply current waveforms at that particular slip. In addition to the comments made in the previous section about the rotor currents, the difference between the measured and the predicted rotor current waveforms at this speed is of a fundamental nature. The shapes of the measured and predicted rotor current waveforms are clearly different and indicate that the actual overlap angle at this speed is considerably larger than the one predicted. This peculiar harmonic effect is adequately catered for in a more detailed model [3] as shown in figure 13. The stator and supply currents are nevertheless predicted fairly accurately.

6. Conclusion

This paper has used two versions of the equivalent circuit to calculate the performance of a chopper-controlled slip energy recovery induction motor drive. The transformer-type EC was used to calculate the steady state drive behavior including efficiency, power factor, real and reactive powers. Satisfactory results were obtained over a wide operating speed range including chopper and inverter control.

The conventional form of the EC was then used to calculate the nonsinusoidal supply, stator and rotor current waveforms. Although both inverter-induced and rectifier-induced ripple was neglected, good correlation was obtained between the predicted and measured results. This implies that the rotor current ripple does not play a significant role in determining those waveforms.

The models produce errors at a speed of 1250 rpm (slip = 1/6) but the calculated supply and stator current waveforms were still fairly accurate. At this slip only the detailed model [3] gives correct results. The results indicate that the drive performance can be accurately calculated with the EC over most of the operating speed range including both chopper and inverter control. The use of the EC avoids the mathematical and numerical complexities associated with solving the nonlinear equations in [3]. Also, the effects of particular rotor harmonics on the stator or supply currents can be investigated, which cannot be easily done with the detailed model.

ACKNOWLEDGEMENTS

The authors acknowledge the help of Professor Alan Jack. P.Pillay would like to thank EPRI, Entergy, LP&L, CLECO and Mobil Refinery, Chalmette for funding his research.

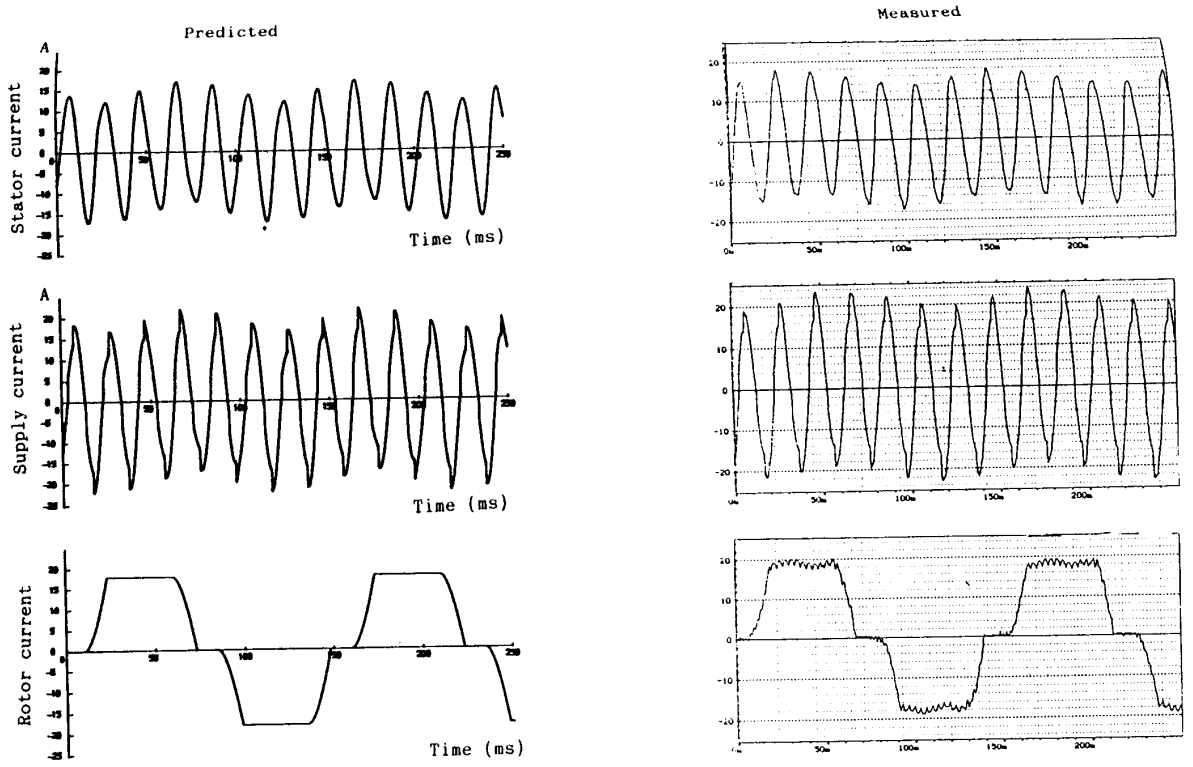

Figure 11. Measured and calculated current waveforms at 1300 rpm

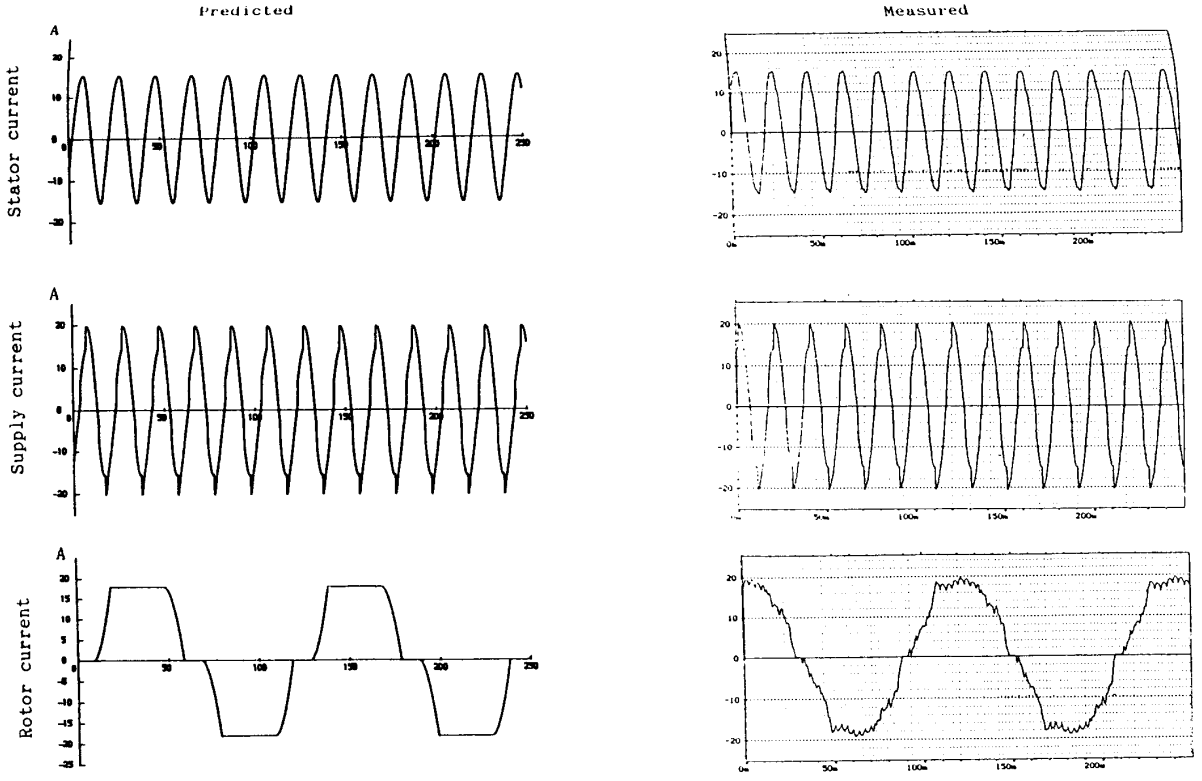

Figure 12. Measured and calculated current waveforms at 1250 rpm

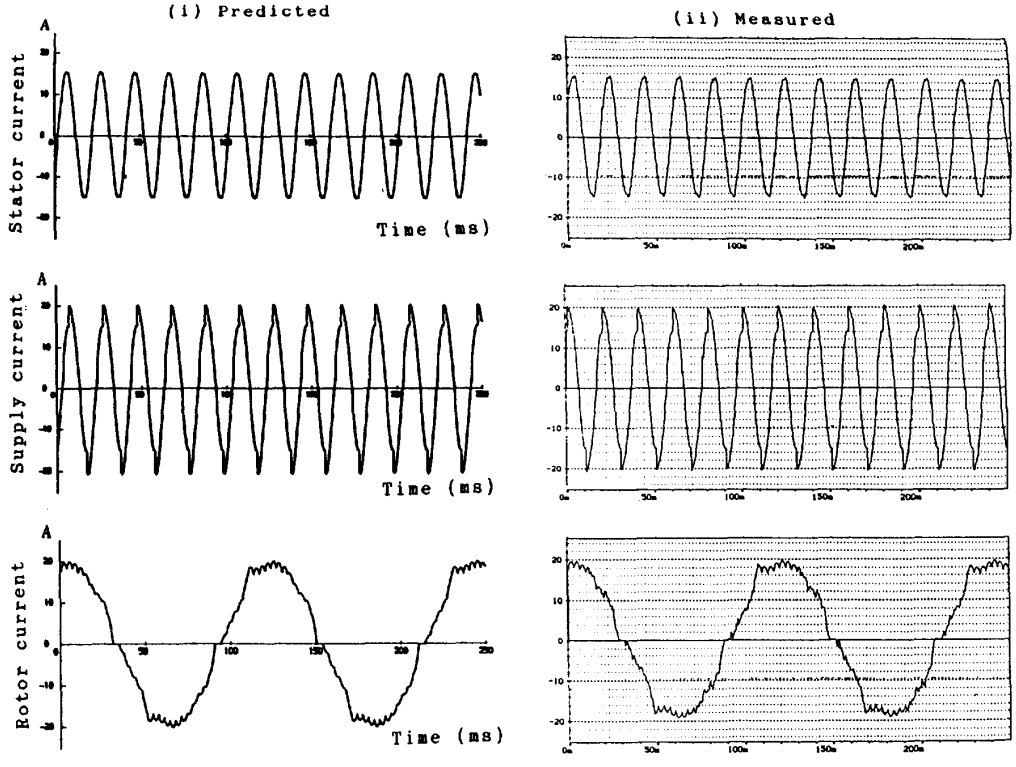

Figure 13. Measured and calculated current waveforms at 1250 rpm

REFERENCES

1. E.Akpinar and P.Pillay, "Modeling and performance of slip energy recovery induction motor drives", IEEE Trans., vol EC 5, No. 1, March 1990, pp 203-210.

2. E.Akpinar and P.Pillay, " A computer program to predict the performance of slip energy recovery induction motor drives", IEEE Trans., vol EC 5, No. 2, June 1990, pp 357-365.

3. L.Refoufi, P.Pillay and M.R.Harris, "A chopper-controlled slip energy recovery induction motor drive", IEEE 1992 PES Summer Meeting, Seattle, Washington.

4. P.C.Sen and K.H.J.MA, "Rotor chopper control for induction motor drive" IEEE Trans., vol IA-11, Jan/Feb 1975, pp. 43-49.

5. A.Lavi and R.J.Polge, "Induction motor speed control with static inverter in the rotor", IEEE Trans., PAS 85, Jan 1966, pp. 76-84.

6. T.Hori, "Secondary excitation of induction motors using rectifier circuits", Trans., IEE Japan, vol 87, Sept, 1968, pp 55-65.

7. B.A.T. Al Zahawi, B.L. Jones and W. Drury, " Analysis and simulation of static Kramer Drive under steady state conditions", Proc IEE, vol 136., Pt B., No. 6, pp. 281-291.

8. D.G.O.Morris, "Some tests of an exact practical theory of the induction motor, " Proc IEE., vol 97, Pt II, pp. 767-778.

9. B.A.T. Al Zahawi, B.L. Jones and W. Drury, "Effect of rotor rectifier on motor performance in slip energy drives", Canadian Electrical Engineering Journal, vol 12., No 1., 1987.

Appendix 1.

7.5 kW slip ring induction motor

V_1 = 415V, 50Hz, V_r = 224.6V line to line at standstill
R_1 = 0.4688 X_1 = 1.643 R_c = 465.12 X_m = 44.65
R_2 = 0.7543 X_2 = 1.643 2 pole pairs

L_d = 4.3 mH R_d = 0.07
C_d = 3535uF L_b = 31mH R_b = 0.07 R_f = 0.0008 V_f = 0.7V